Mohammadiha and Ghariblu *International Journal of Mechanical and Materials Engineering* (2016) 11:8
DOI 10.1186/s40712-016-0061-3

International Journal of Mechanical and Materials Engineering

ORIGINAL ARTICLE Open Access

Multi-objective optimization of functionally graded thickness tubes under external inversion over circular dies

Omid Mohammadiha* and Hashem Ghariblu

Abstract

This paper optimizes the crushing response and energy absorption of functionally graded thickness (FGT) inversion tubes using the multi-objective optimization method. The numerical results, which are validated by the experimental tests, confirm that optimizing geometry of FGT inversion tube improves energy absorption capacity with respect to ordinary uniform tube UT with the same weight. Our study shows that the die radius r, coefficient of friction μ_d between the die and tube, and thickness distribution function have great influence on the responses of FGT inversion tubes. The specific energy absorption (SEA), peak crushing force P_{max}, and dynamic amplification factor (DAF) are selected as the objectives of crashworthiness optimal design. Finally, the weighted average method, multi design optimization (MDO) technique, constrained single-objective optimization, and geometrical average method were employed to find the optimal configuration of the proposed inversion tube. The results give new design ideas to improve crashworthiness performance of inversion tubes.

Keywords: Inversion tube, Functionally graded thickness, Finite element, Multi-objective optimization

Background

Energy crisis and environmental concerns place higher requirement to decrease the weight of vehicles and achieve a highest possible safety and quality with minimum cost. In the last few decades, there has been a continuous focus on design optimization as a primary requirement in the design of automotive structures. Lightweight materials, such as aluminum and magnesium alloys, are gradually finding their place in vehicle engineering (Miller et al. 2000). Thin-walled structures are widely used to dissipate the vehicle's kinetic energy in terms of plastic deformation in collisions. Many applications employ thin-walled tubes to enhance the crashworthiness of structure such as energy absorption devices at the front of cars and trains (Marsolek & Reimerdes 2002), aircraft sub floor structures (Bisagni), and rollover protective structures (ROPS) of heavy vehicles, such as bulldozers and tractors (Ahmad & Thambiratnam 2009a). Thin-walled tubes with different geometries and materials are commonly used to absorb kinetic energy through plastic material deformation. The widespread use of thin-walled tubes as energy absorbers is due to their good performance under dynamic loading, availability, low manufacturing cost, and efficiency. Numerous efforts have been made in the past decades to improve the crashworthiness performance of the crush absorber tubes, such as foam filled tubes (Hanssen et al. 2000; Ahmad & Thambiratnam 2009b; 2009c; Aktay et al. 2008; Mirfendereski et al. 2008), introducing different patterns (Zhang et al. 2007), grooves (Zhang & Huh 2009; Saleh ghaffari et al. 2010), multi-cells (Zhang & Zhang 2013; Zhang & Zhang 2014), and functionally graded structures (Mohammadiha & Ghariblu 2016; Sun et al. 2010). Relative merits of conical tubes with graded thickness subjected to oblique impact loads are investigated by Zhang (Zhang & Zahng 2015).

Inversion is a mode of plastic deformation which develops when a thin-walled tube is compressed between a flat plate at one end and filleted die at the other (Al-Hassani et al. 1972a; Reddy 1992a). Therefore, analysis of external inversion process is equally important for manufacturing technology as well as for impact and crashworthiness

* Correspondence: omid_mohammadiha@znu.ac.ir
Department of Mechanical Engineering, University of Zanjan, Zanjan, P. O. Box 81746-73441, Iran

studies. Tube curling mode is a case of forming behavior between flaring and buckling failures; only meeting certain forming conditions can the tube curl to produce an axially symmetric second wall (Reddy 1992a). Recently, many applications of inversion tubes have been made, such as force actuating collapsible steering wheels, cushioning air drop cargo, helicopter seats, and soft landing of spacecraft (Guist & Marble 1966). Experimental studies and theoretical analysis on tube inversion have been conducted by many researchers in the recent decades. Al-Hassani et al. (1972b), Reid (Karagiozova et al. 2000), and Reddy (1992b) made experimental investigations and theoretical analyses for the deformation behavior and forming load of external inversion. Miscow and AL-Qureshi (1997) studied the theoretical and experimental studies of the static and dynamic inversion process in circular tubes. This theoretical analysis is valuable as the first formula that predicts the axial force versus the axial displacement during the inversion process. But theoretical curve that sketched based on Miscow's theory shows an intensive increment at the onset of loading with a large difference, comparing the experimental curve. The effects of strain rate and inertia during dynamic free inversion process were further investigated by Colokoglu and Reddy (1996). However, the prediction process is very complicated and generally, theory and experiments have not been in acceptable agreements with each other. Accordingly, the predicted quasi-static inversion load is significantly lower than experimental value while the predicted dynamic mean load is overestimated. Chirwa (1993) investigated the plastic collapse of a tapered thin-walled metal Inver buckle energy absorbing tube subjected to axial impact. In this work, predicted specific energies and loads of collapse modes had been in good agreement with the experimental results. Recently, Masmoudi et al. (2016) carried out numerical and experimental analyses of external curling of thin-walled round tubes. Their model provides an accurate prediction on the forming kinematics and the deformed shape.

Reviewing the literature presents an effective way to increase the energy absorption of a structure, which is to harden the materials and simultaneously design the optimal structures. Up to now, the multi-objective optimization of functionally graded thickness (FGT) inversion tubes has never been investigated or presented elsewhere, even though optimal shapes of die and tube are very important in the crashworthiness of external inversion of tubes.

The aim of this study is to address the crashworthiness design issues of the various FGT inversion tubes under axial loading through the several quasi-static tests by following the multi-objective optimization procedure. A finite element (FE) model is developed to simulate the graded thickness in FGT tubes, and this FE model is validated through experimental tests. An integration of finite element modeling (FEM) with the response surface method (RSM) for design of experiments (DOE) was employed for generating the design guidelines for such inversion tube as energy absorbing devices. Finally, multi-objective optimization for different FGT are carried out, while specified energy absorption and peak force are selected as objective functions. Another focus was the relative merits of the optimized inversion tubes under dynamic loads, which has been raised by some pioneer researchers (Miscow & AL-Qureshi 1997) and not yet been disclosed. The results will demonstrate that the optimal FGT inversion tubes can be recommended as efficient energy absorbers. The primary outcome of this study is new design optimum information on the energy absorption performance of inversion tubes.

Methods

Objective functions of structural crashworthiness

To evaluate the energy-absorbance of structures and optimize their performance, it is necessary to define the crashworthiness objective functions of energy absorber. The ultimate objective of a crashworthy structure is to minimize occupant injuries and trauma. The specified energy absorption (SEA) is defined as the area under the load-displacement curve per unit mass represented as follows:

$$\mathrm{SEA} = \frac{\int_0^d F dx}{m_c} = \frac{E}{m_c}, \tag{1}$$

where, m_c is the total mass of the component and E is the energy absorbed. SEA is a key indicator to distinguish energy absorption capabilities for various structures and weights. The total strain energy absorbed by the structure during the deformation includes not only the elastic component but also the plastic strain energy.

On the other hand, the peak crushing force P_{max} is sometimes considered one of the critical design objectives to prevent the occupant's body from severe biomechanical injury (Qiao et al. 2004). In the load-displacement curve, the peak crushing force P_{max} is defined as the maximum collapse load during the crushing strike. In this study, SEA and P_{max} are selected as the independent parameters in multi-objective optimization.

Finite element models of FGT inversion tubes

As illustrated in the schematics in Fig. 1, two different structural configurations, namely UT and FGT tubes, are studied in this paper. The mathematical expression for grading thickness distribution of FGT tube is given by

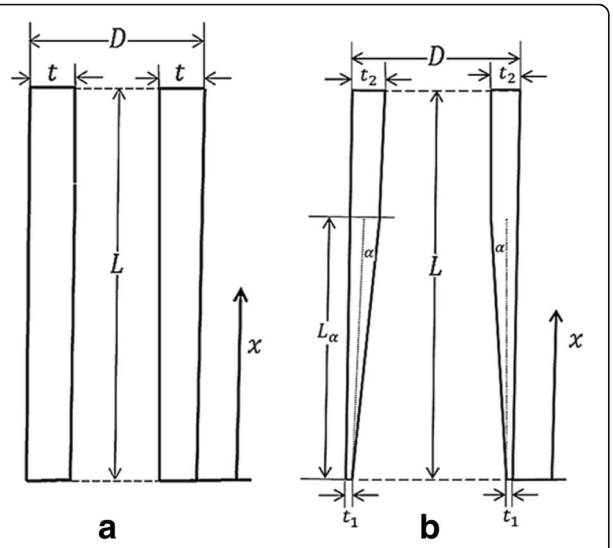

Fig. 1 Schematic view of the test specimens. **a** Uniform tube UT. **b** Functionally graded thickness FGT tube

$$T(y) = t_1 + (t_2 - t_1)\left[\frac{x}{L_\alpha}\right]^m. \tag{2}$$

Here, all of the tubes have the same baseline dimensions with length $L = 85$ mm and outer diameter $d = 50$ mm. It is first assumed that the FGT tubes have a linearly graded thickness from $t_1 = 1$ mm to $t_2 = 2$ mm, and the UT tubes have an equivalent thickness of $t = 2$ mm. Also, the terms α and L_α in Fig. 1 are the angle and length of tube section with distributed thickness. Meanwhile, x is the distance from bottom to the height L_α and m is the order of thickness distribution, with $m = 1$ for linear variation of tube thickness.

As shown in Fig. 1, L_α in specimens for three different angles can be calculated as follows:

$$L_\alpha = \frac{t_2 - t_1}{\tan\alpha}. \tag{3}$$

So, L_α for three different angles are calculated as

$$L_{\alpha=1^\circ} = 57.2 \text{ mm};\quad L_{\alpha=2^\circ} = 28.63 \text{ mm};$$
$$L_{\alpha=3^\circ} = 19.08 \text{ mm}.$$

Developing an accurate FE analysis, proper selection of the impact modeling technique will have great contribution on crashworthiness analysis. Here, the crush behavior of UT and FGT tubes is studied to predict their main crashworthiness features as function of the tube material and geometrical parameters. The FE analysis is employed to find these behaviors for various cases which are difficult and expensive to perform by experimental tests. The finite element models of the tubes were developed with the use of commercial explicit finite element code LS-DYNA. Aluminum alloy is modeled by applying the piecewise linear elastic-plastic material model with the constitutive equation of strain hardening as (Karagiozova et al. 2000):

$$\dot{\varepsilon} = D\left(\frac{\sigma_0'}{\sigma_0} - 1\right)^q, \tag{4}$$

in which

σ_0' is the dynamic flow stress at a uniaxial plastic strain rate, σ_0 is the associated static flow stress, and the constants D and q are material parameters. These parameters are selected for aluminum 6061 as $D = 1{,}288{,}000\, s^{-1}$ and $q = 4$ (Karagiozova et al. 2000). The yielding function is defined by the von-Mises yielding criterion as:

$$\varphi = \frac{1}{2} S_{ij} S_{ij} - \frac{\sigma_y}{3}. \tag{5}$$

Where S_{ij} and σ_y are the deviatoric stress and the current radius of the yield surface. As illustrated in Figs. 2 and 3, the full section FGT and UT tubes are modeled by the quadrilateral Belytschko-Tsay shell element with four nodes and three integration points considered throughout the thickness. Top and bottom plates modeled as rigid bodies. It is assumed that the bottom die is fixed and the top plate only moves in longitudinal direction and has one degree of freedom. The optimum mesh size for each simulation is obtained after performing the mesh sensitivity analysis. It indicates that an element size of 3 mm (3200 elements in FE model) is adequate to produce suitable results. In other words, the mesh size is suitable when the obtained results are logical for crush simulation and do not change drastically.

The automatic single surface contact algorithm is used to account the contact force between the crush zone surfaces or metal folds. The node to surface algorithm models the contact between the rigid plate (die) and the crushed components. The friction coefficients at the different interfaces have been taken $\mu = 0.2$. In all simulations, the die radius is $r = 3$ mm. To obtain the appropriate value of friction factor μ_d between die and tube interface, various values for μ_d were tested. It is seen that when $\mu_d = 0.02$ was utilized, the load-displacement curves and deformed shapes of tubes are similar to the experimental tests. Therefore, the value of friction coefficient $\mu_d = 0.02$ assumed for subsequent study.

Material properties

The circular aluminum alloy AA6061 tubes utilized for experimental tests. To obtain tubes exact stress-strain curve and mechanical properties, three similar specimens prepared from tubes in longitudinal direction based on ASTM standard tensile test (Fig. 4) (ASTM Standard E8/E8M-08 2003). The strain rate was 2.77 ×

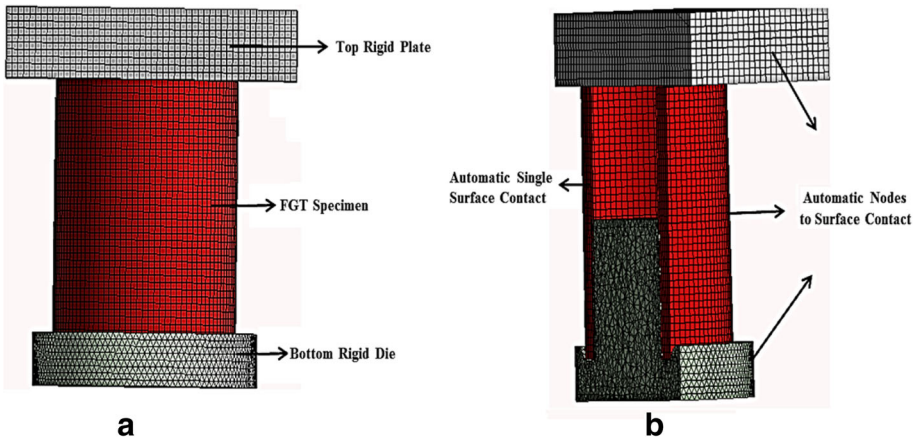

Fig. 2 The details of representative finite element model for FGT inversion tube with die and uniform circular without die. **a** Overall view. **b** Cross-sectional view

$10^{-3}\,s^{-1}$. The mechanical properties of aluminum alloy AA6061 are tabulated in Table 1.

Validation of finite element models

The FE result of the UT tube without die and FGT tubular specimens under axial loading condition compared and validated by experimental results. Quasi-static compression tests of specimens have been done using the 250 kN standard tensile-compression test machine. The top plate feed rate is considered as 3 mm/min with maximum 40 mm progress. Friction plays a significant role to ensure the process of tube inversion to deform. Grease based on lithium soap was used during experiment to reduce the friction factor and preventing folding mode of tube crush. The die surface and inner area of the tubes has been lubricated with grease before conducting the experiments. Three different tube profiles with angles $\alpha = 1°$, 2°, and 3° are investigated here and three specimens are prepared for each case (Fig. 5).

As depicted in Figs. 6 and 7, in order to compare FGT and UT tube crush responses with each other, only FGT tubes with linear thickness variation with angles $\alpha = 1°$, 2°, and 3° are tested. Then, by optimization, the FE model is employed to consider with different geometries for FGT tubes.

The final crushed shape of UT and FGT tubes is shown in Fig. 8a–d. In Fig. 8a, both experimentally and numerically, it is seen that in the UT tube without die the folding begins from the upper section and continues with stacking more folding during the crushing. Also, as depicted in Fig. 8b–d, different deformation modes are observed in FGT tubes with linearly variable thicknesses. In all three FGT specimens with angles $\alpha = 1°$, 2°, and 3° tubes, thickness starts from $t_1 = 1$ mm at bottom side to maximum $t_2 = 2$ mm at height L_α (Fig. 1). Because of relatively smaller cross section of the FGT tubes in the bottom side, compression load results in higher stress rates at this side and deformation of all FGT specimens start from

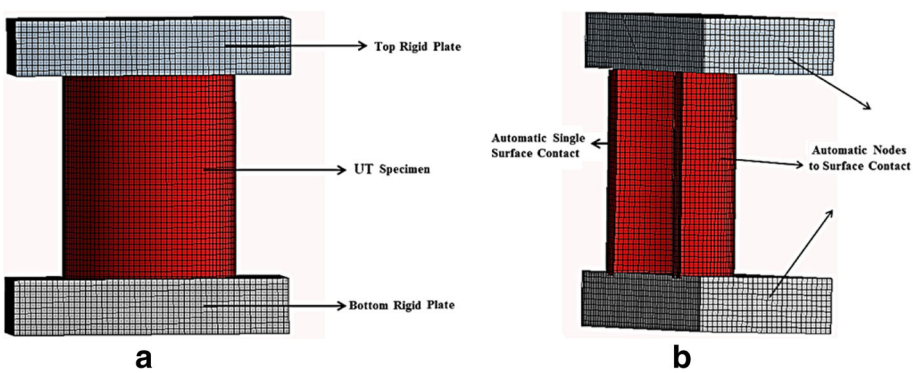

Fig. 3 The details of representative finite element model for UT tube without die. **a** Overall view. **b** Cross-sectional view

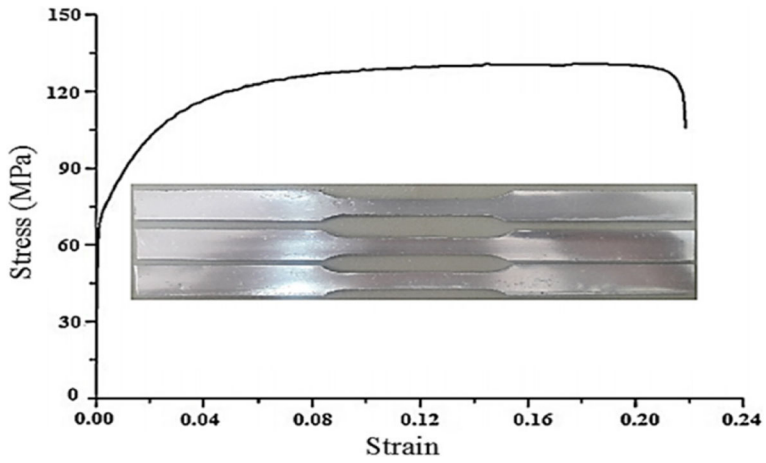

Fig. 4 Engineering stress-strain curve of aluminum alloy AA6061

the bottom by inversion of tubes. But, approximately, after reaching to the height of L_α, inversion process changes to folding of tubes. Therefore, complete inversion of tube only occurs in the FGT tube with $\alpha = 1°$ with $L_{\alpha=1°} =$ 57.2 mm that is greater than 40 mm maximum compression progress. The comparison between load vs. displacement between experimental and FE simulation is shown in Fig. 9. The predicted load-displacement curve shows acceptable agreement with experimental curves.

For better comparing the results of finite element energy absorption characteristic of UT tube and FGT tube with the experimental results, various results are presented in Table 2. In Table 2, P_{max} (peak load), P_m (mean load), E and SEA in various tube geometries are calculated by FE simulation and compared with the experimental tests. The FE simulation results indicate acceptable agreement with experiments.

From experimental results represented in Fig. 9 and Table 2, it is seen that load-displacement curve in the complete inversion process for FGT tube with $\alpha = 1°$ is smoother than the UT tube with folding crush behavior, and meanwhile SEA = 43.9 and mean force $P_m = 39.3$ kN of FGT tube with $\alpha = 1°$ is meaningfully more than SEA = 32.4 $P_m = 28.1$ kN for UT tube with the same overall dimensions. Beside on, initial peak force in the FGT tubes is lower than in the UT tube. Therefore, using optimal FGT tubes guarantees full inversion process with better crush characteristics and behavior. The validated FE model will be further used for optimization designs in the following sections.

Multi-objective optimization design

Design methodology

While the effect of various parameters on crushing response has been addressed in the previous sections, it is still unknown how to design specific best designs for thin-walled circular inversion tubes under the axial loading. The die radius r, coefficient of friction μ_d, and order of thickness distribution have great influence on the responses of FGT inversion tubes. In this section, a fundamental optimization problem is solved and the optimum values of these design variables are obtained. The approximate function relation that predicts the amount of desired objectives was obtained from the RSM. RSM is a method for constructing functions that describe the correlation between the design variables based on the FE simulation results. The improved RSM flowchart is shown in Fig. 10, where the experimental designs are generated through saturated Latin hypercube design (LHD) points (Liao et al. 2008). In order to construct a fourth-order RSM model, the number of $(r_v + 1)^s$ design points selected for the design variables. In this optimization study, r_v (order of the polynomial objective function) and s (the number of design variables) are correspondingly assigned to each optimization problem. Design variables continuously increase with an increase of 0.1, from 0 to 10 for m, 1 to 3 mm for t, and 2 to 6 mm for r. This increase for the angle α in linear thickness distribution is 0.1° from 1° to 3°. In automotive scenarios, the peak load P_{max} and SEA are critical to the occupant

Table 1 The tensile mechanical properties of aluminum alloy AA6061

Mechanical properties	Young's modulus E	Yield strength $\sigma_{0.2}$	Ultimate tensile strength	Poison ratio ϑ	Failure strain %
Value	68.4 GPa	75.8 MPa	130 MPa	0.3	22

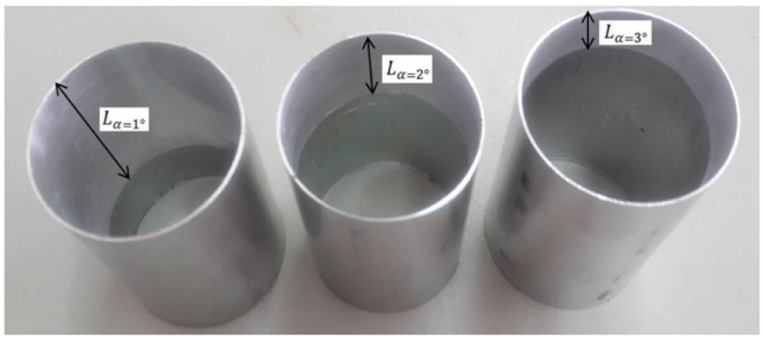

Fig. 5 Specimens of *f* FGT tubes for three different angles$\alpha = 1^\circ, 2^\circ$, and 3°

survival rate when impact occurs. An overly high P_{max} and less SEA often lead to severe injury or even death of occupant. In this study, these parameters are selected as objective functions in the multi-objective optimization framework.

Error evaluation of the surrogate model

As indicated in the previous section, RSM model constructed through LHD point's selection. The numerical errors in the fitted regression model can be caused by the selection of basic functions, selection of sampling points and the least square and includes effects such as random and measurement errors on the response (Liao et al. 2008). In this study, the two central composite design (CCD) and LHD selection methods were employed and the error obtained from these methods was compared with the different polynomial RS models. The statistical parameters used for evaluating the model fitness the error sum of square (SS_E), the total sum of square (SS_T) calculated as

$$SS_E = \sum_{i=1}^{M} \left(y_i - \tilde{y}_i\right)^2, \tag{6}$$

$$SS_T = \sum_{i=1}^{M} (y_i - \overline{y}_i)^2, \tag{7}$$

where y_i the numerical solution obtained from FE, $\overline{y}_i$ is the mean value of FE, and y_i represents approximation based on the response surface model. Relative error (RE), root mean square (R^2), adjusted root mean square (R^2_{adj}), and root mean square error (RMSE) are sequentially given by the following relations (Zhang & Zhang 2014)

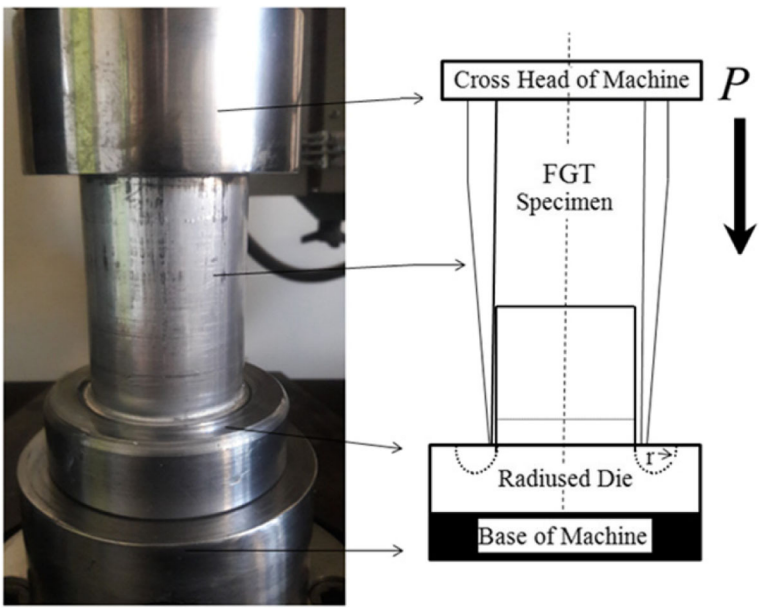

Fig. 6 Experimental set up and the die used for studying the external inversion process of FGT tubes

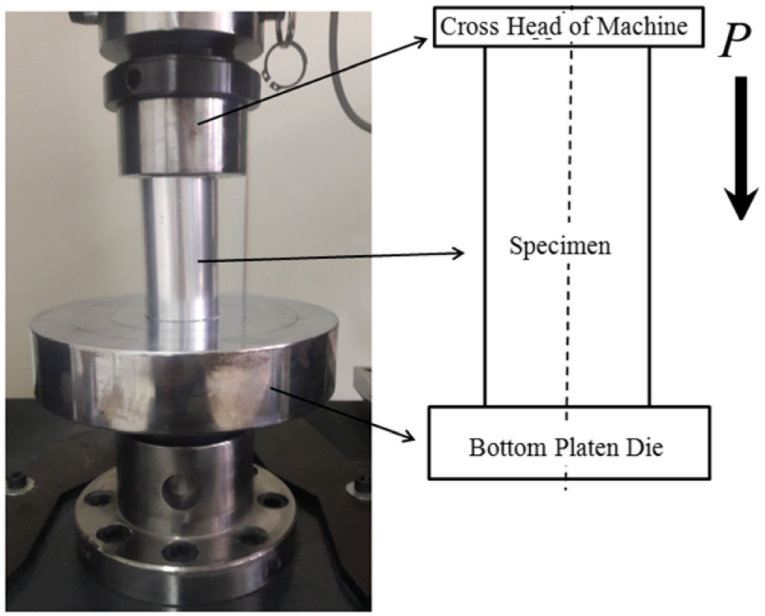

Fig. 7 Experimental setup used for studying uniform thickness tube without die

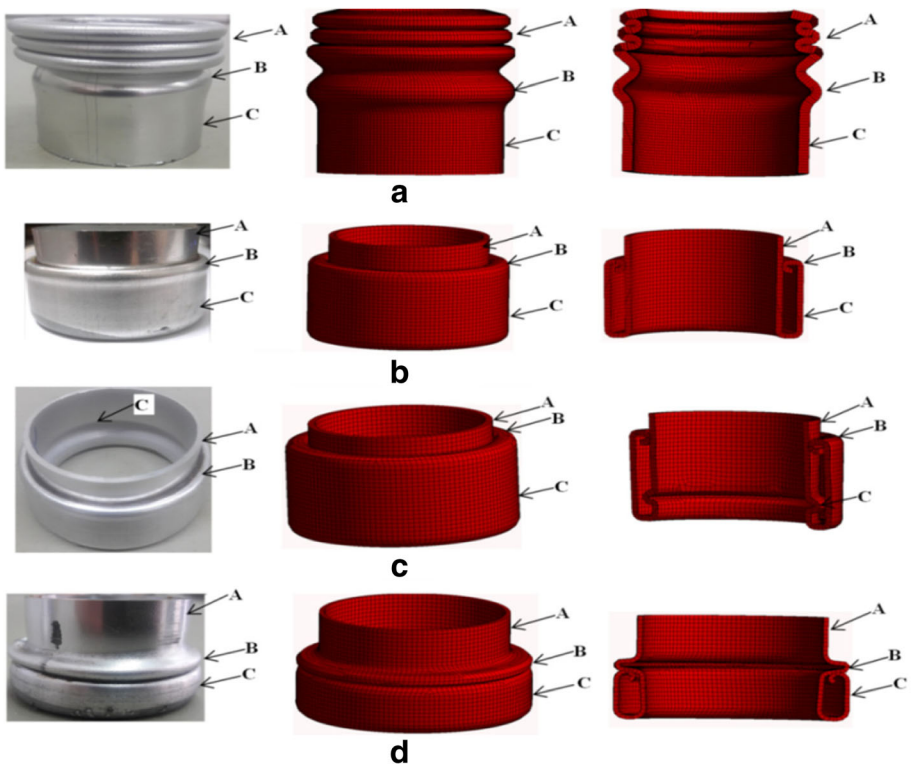

Fig. 8 Experimental and FE simulation deformation pictures. **a** UT tube. **b** FGT tube with lathe angles $\alpha = 1^{\circ}$. **c** FGT tube with lathe angles $\alpha = 2^{\circ}$. **d** FGT tube with lathe angles $\alpha = 3^{\circ}$

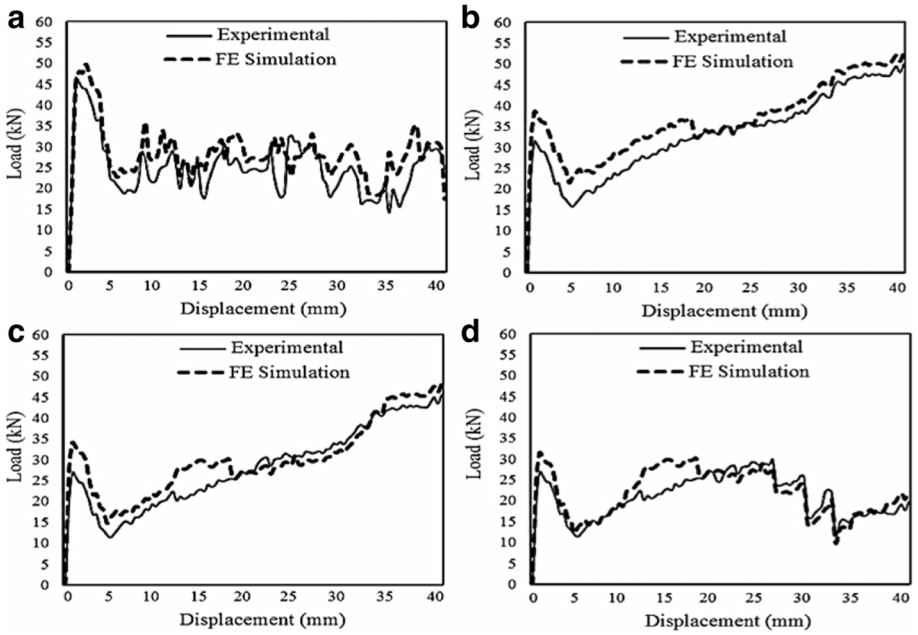

Fig. 9 Experimental and simulation load-displacement curves. **a** UT tube. **b** FGT tube with lathe angles α=1°. **c** FGT tube with lathe angles α=2°. **d** FGT tube with lathe angles α=1°

$$\mathrm{RE} = \frac{\tilde{y}_i - y_i}{y_i}, \tag{8}$$

$$R^2 = 1 - \mathrm{SS_E}/\mathrm{SS_T}, \tag{9}$$

$$R_{\mathrm{adj}}{}^2 = 1 - \left(1 - R^2\right)\frac{M-1}{M-p-1}, \tag{10}$$

$$\mathrm{RMSE} = \sqrt{\frac{SS_E}{M-p-1}}, \tag{11}$$

where p is the number of none constant terms in the RS model and M is the number of design sampling points. Relatively higher values of R^2 and R^2_{adj} and relatively smaller values of RMSE and RE indicate the better agreement between FE and response surfaces model. The results of the error evaluation are tabulated in Table 3 (a) and (b) for SEA (m, μ_{d}) analysis carried out by CCD and LHD selection methods. One can see from the result that quadratic polynomial function constructed by LHD method provides the best fitness.

Optimization of die radius *r* and angle *α* for linear thickness variation

Multi-objective optimization problem can be expressed in terms of the linear weighted average of objective functions as (Hou et al. 2008):

$$\begin{cases} \text{Minimize } Fw = (1-w)\dfrac{f_1^*}{f_1} + w\dfrac{f_2}{f_2^*}, \\ \text{St } w \in [1,0] \text{ and } x^l \leq \times \; x^u \end{cases} \tag{12}$$

in which $f_1 = SEA$, $f_2 = P_{\max}$, and f_1^*, f_2^* correspondingly are the given normalizing values of SEA and $P_{\max}$. Regarding the multi design optimization (MDO), x represents the design variables r and α. Additionally, superscripts l and u, respectively, indicate the lower and upper bound of design variables, while w is the weight factor to emphasize the effectiveness of these two objectives. The optimal

Table 2 Experimental and FE simulation results for various types of tubes

Tube case	$P_{\max}$(kN)			P_{m}(kN)			E(kJ)			SEA(kJ/kg)		
	Exp.	FE	Diff. (%)	Exp.	FE	Diff. (%)	Exp.	FE	Diff. (%)	Exp.	FE	Diff. (%)
UT	47.9	52.4	8.5	28.1	33.4	15.8	1.6	1.9	15.7	32.4	38.5	15.8
FGT (α=1°)	47.4	53.9	12.6	39.3	42.9	7.2	2.1	2.5	16	43.9	48.6	9.6
FGT (α=2°)	43.6	49.2	11.3	37.8	45.2	16.3	1.9	2.3	17.3	38.2	42.3	10.7
FGT (α=3°)	28.4	33._6	15.4	31.1	35.6	7.5	1.8	2.1	14.2	37.6	41.9	10.2

Exp experimental results, *FE* finite element results, *Diff* difference

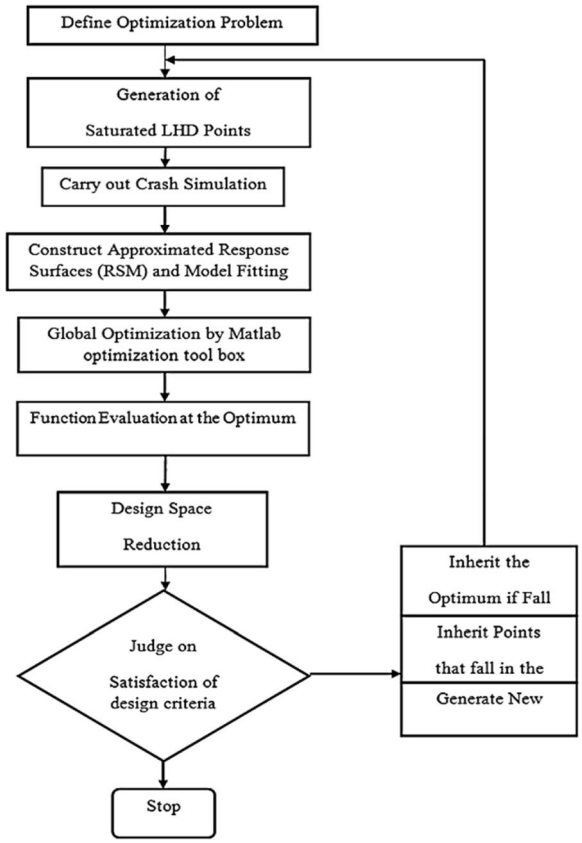

Fig. 10 The flowchart of the improved RSM

results of Pareto's points can be determined by changing parameter w in Eq. (12). It should be noted that Pareto sets provide the designer with a large number of optimal solutions. The setup of Pareto sets is crucial to fully understand the solution space for these two different design criteria.

Solving the optimization problem, the maximum SEA value is 56.4 kJ/kg and minimum of $P_{\max}$ is 32.4 kN which is obtained at point ($r = 3.43$ mm, $\alpha = 1.41°$).The Pareto sets for FGT is plotted in Fig. 11. Because of the

Table 3 Accuracy of different polynomial RSM models based on (a) CCD and (b) LHD

RS model	R^2	R^2_{adj}	RMSE	RE interval (%)
(a)				
Quadratic polynomial	0.9957	0.9942	0.0921	[−2.18,2.24]
Cubic polynomial	0.9966	0.9956	0.0723	[−1.03,2.31]
Quartic polynomial	0.9984	0.9977	0.0316	[−0.78,1.17]
(b)				
Quadratic polynomial	0.9990	0.9990	0.0893	[−1.76,2.04]
Cubic polynomial	0.9992	0.9990	0.0714	[−0.74,1.58]
Quartic polynomial	0.9999	0.9997	0.0292	[−0.39,1.08]

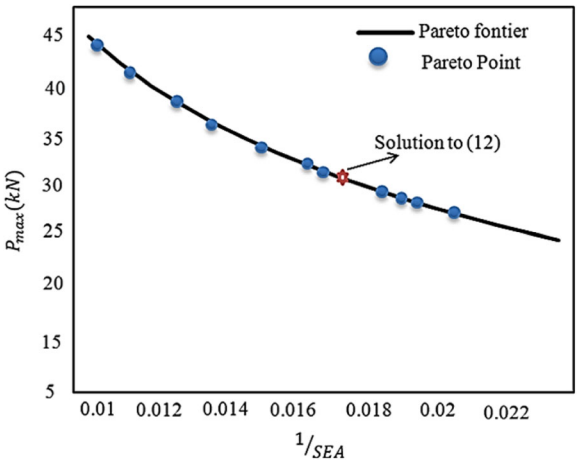

Fig. 11 The Pareto sets for optimum FGT inversion tube

complex nature of design objectives and variables, the convexity of Pareto space is not guaranteed. However, convexity of all plotted curves signifies the effectiveness of using linear weighted method to explore for multi-objective optimization (Masmoudi et al. 2016). By setting the design variables to the optimum point, a numerical verification analysis is conducted and load-displacement curve for the optimal design are given in Fig. 12. The SEA value is 54.1 kJ/kg and $P_{\max}$ is 33.8 kN at the optimum point. The difference between the predicted value and verification value is about 4 %, which shows a very good approximation.

Design optimization for coefficient of friction μ_d and exponent gradient m

In order to find the best tube configuration, the MDO procedure (Zarei & Kroger 2008) has been applied to

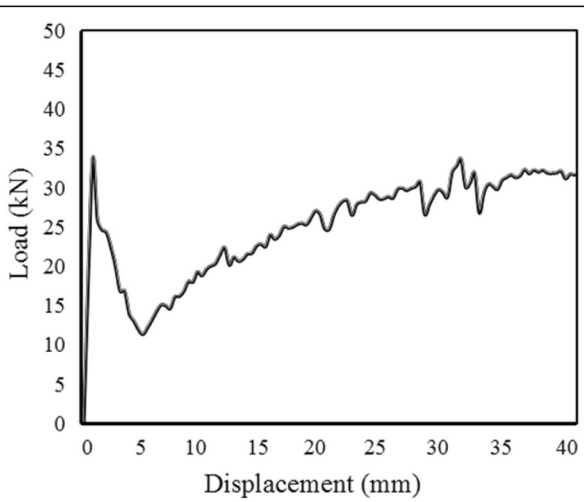

Fig. 12 Load-displacement curve for optimal design of FGT inversion tube

maximize SEA and minimize P_{max} of the FGT tubes with coefficient of friction μ_d and exponent gradient m as design variable. The first design variable space for m and μ_d was selected based on the experience and FE simulations that is performed by the authors. Then, the approximation sub problem was solved, employing the genetic algorithm optimization method. Additionally, the second design cycle was constructed and the corresponding optimum values were determined. Investigation on the optimum value of design variables reveal that these values are near to upper or lower bound; accordingly, the variables are shifted to lower or higher values. These cycles continue to a point where the objective function is improved for the crashworthiness. The optimum value of design variables calculated from MDO are given in Table 4.

Design optimization for die radius *r* and thickness exponent gradient *m*

It is assumed that the thickness exponent gradient m is positive constant that must be adjusted to obtain a certain type of power law variation in FGT inversion tubes. The achieved optimization results in previous section reveal that coefficient of friction $\mu_d = 0.031$ has better crashworthiness performance than other values. To design a suitable geometry for inversion die in this section, the design parameters for optimization process are selected as m and r. With the explicit formulation of SEA (m, r) and P_{max} (m, r), the two constrained single-objective optimization in the multi-objective optimization framework defined as:

$$\begin{cases} Maximize\ SEA\ (m,r) \\ P_{max}\,(m,\ r) \le 35\,kN \\ St \quad m^l \le m \le m^u \\ \qquad r^l \le r \le r^u \end{cases} \tag{13}$$

$$\begin{cases} Minimize\ P_{max}\ (m,\ r) \\ SEA\,(m,\ r) \ge 55\,kJ/kg \\ St \quad m^l \le m \le m^u \\ \qquad r^l \le r \le r^u \end{cases}, \tag{14}$$

where, l and u superscripts represent the lower and upper limits of the design parameters, respectively. Applying "FMINCON," a constrained nonlinear multivariable optimization function in MATLAB software, the optimal results of Eqs. (13) and (14) are achieved and correspondingly summarized in Table 5. Additionally, from Table 5, the optimization results for constrained single-objective optimization and optimum magnitudes m and r can be found in both the *SEA* design and the peak crushing force design.

The SEA (m, r) and P_{max} (m, r) are the specific energy absorption and the peak load, determined with respect to the grading exponent m and die radius r. These objective parameters are drawn in Figs. 13 and 14.

Dynamic loading

Quasi-static test is not able to express actual crashworthy structure behavior. It is also interested to quantify the effect of the various inversion parameters on the dynamic response of FGT inversion tubes and compare them with the quasi-static response. The explicit finite element procedure was used to analyze the dynamic response of UT and FGT inversion tubes subjected to axial impact loading. The calculated absorbed energy is compared with the corresponding results obtained for quasi-static simulation. In this study, dynamic amplification factor (DAF) was used to consider the dynamic effect of crash. The term DAF relates quasi-static and dynamic responses to each other and is defined as the ratio of the absorbed energy under dynamic loading to the absorbed energy under quasi-static loading (Ahmad & Thambiratnam 2009b). The effect of strain rate on the yield stress is described by Eq. (4), whose parameters are mentioned in the "Material properties" section for D and q. Here, the influence of nonlinear thickness distribution of FGT tubes under various loading velocities is established. The FGT tubes main dimensions are $t_1 = 1$ mm, $t_2 = 3$ mm, die geometry $r = 4$ mm, and coefficient of friction $\mu_d = 0.03$. Figure 15 shows significant effect of exponent gradient m on the DAF for both UT and FGT tubes. The results show that dynamic energy absorption

Table 4 Optimum friction μ_d and exponent gradient m obtained through MDO for FGT inversion tube

Number of cycle	Design parameter interval	Optimal exponent gradient m	Optimal friction μ_d	SEA (kJ/kg)	P_{max} (kN)
1	$3 < m < 4$ $0.01 < \mu_d < 0.02$	4	0.02	44.16	49.51
2	$4 < m < 5$ $0.02 < \mu_d < 0.03$	5	0.029	48.2	43.29
3	$5 < m < 6$ $0.03 < \mu_d < 0.04$	5.8	0.031	51.3	39.43
4	$6 < m < 8$ $0.03 < \mu_d < 0.035$	7.3	0.03	54.6	35.18
5	$7 < m < 8$ $0.03 < \mu_d < 0.033$	7.3	0.031	57.9	33.2

Table 5 Optimization results of SEA for FGF filled conical tube with peak crushing force constraint

Type of optimization method	Optimal design variable	SEA (kJ/kg)	F_{max}(kN)
Peak load constraint	$m = 7.33$, $r = 3.13$ mm	64.8	34.2
SEA constraint	$m = 7.41$, $r = 3.18$ mm	58.2	31.7

property of concave distribution of thickness $m > 1$ is better than the convex pattern $m < 1$. This effect can be related to the smooth rising in the load displacement of the FGT tube, rising the interaction between the tube and die, and the higher plastic energy damping of concave FGT structures.

Design optimization of DAF for coefficient of friction μ_d and exponent gradient m

As shown in the previous section, the thickness distribution has great influence on the dynamic responses of FGT inversion tubes, and in this section, a fundamental optimization problem is solved and the influences of thickness variables on DAF of the structure are analyzed. In order to find the best tube configuration, MDO procedure has been applied to maximize DAF(m, μ_d) and minimize dynamic $P_{\max}(m, \mu_d)$ of the FGT tubes with coefficient of friction μ_d and exponent gradient m as design variable. The optimum value of design variables calculated from MDO is given in Table 6. Crashworthiness optimization for FGT inversion tube shows that nonlinear concave thickness distribution $m > 1$ is found to show the maximum efficiency.

Design optimization of DAF for die radius r and exponent gradient m

The influence of die radius and exponent gradient m on dynamic response of FGT inversion tube is analyzed based on the approximate function derived by surrogate model. In order to find the best inversion tube configuration, the geometrical average method has been applied to maximize DAF(m, r) and minimize dynamic $P_{\max}$ (m, r) of the FGT tubes with coefficient of die radius r and exponent gradient m as design variable. Based on optimization study carried out in the "Design optimization of DAF for coefficient of friction μ_d and exponent gradient m" section, coefficient of friction μ_d is selected 0.033.

In the geometrical average method, the cost function of relative efficiency of each objective is constructed in terms of a geometrical average as (Hou et al. 2008):

$$\begin{cases} \text{Minimize } F_g = \sqrt{d_{\text{DAF}} d_p} \\ St \quad x^l \le x \le x^u \end{cases} . \tag{15}$$

To maximize DAF, the efficiency coefficient d_{DAF} is expressed in terms of a relative distance from the lower bound, through:

$$d_{\text{DAF}} = \frac{f_{1(x)} - f_1^l}{f_1^u - f_1^l} . \tag{16}$$

And to minimize the peak crushing force, the efficiency coefficient d_p is written as follows:

$$d_p = 1 - \frac{f_{2(x)} - f_2^l}{f_2^u - f_2^l} , \tag{17}$$

where f^l and f^u, correspondingly, are the lower and upper bounds of the objective function in the design

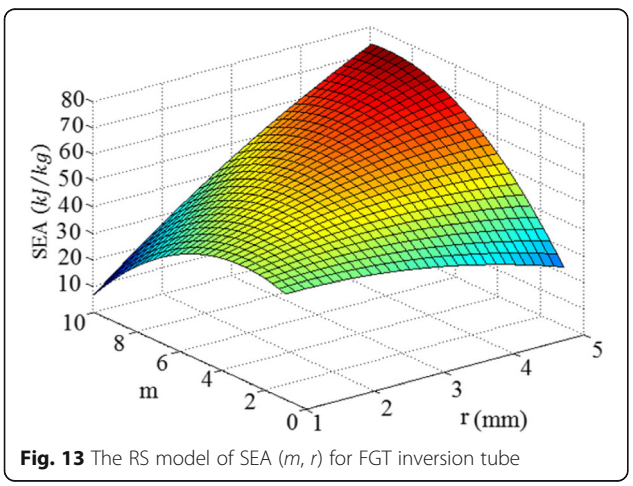

Fig. 13 The RS model of SEA (m, r) for FGT inversion tube

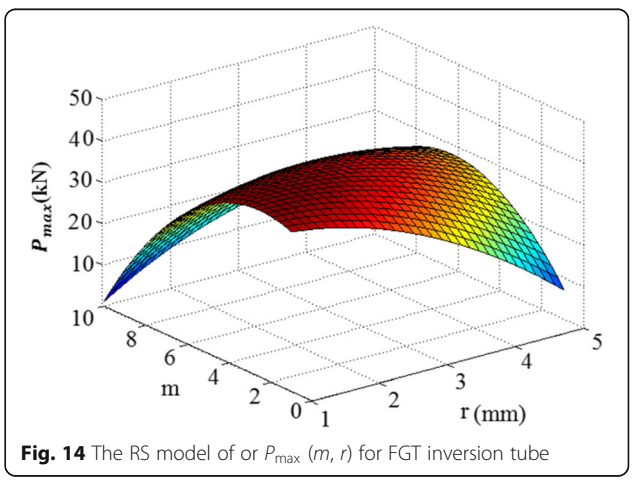

Fig. 14 The RS model of or $P_{\max}$ (m, r) for FGT inversion tube

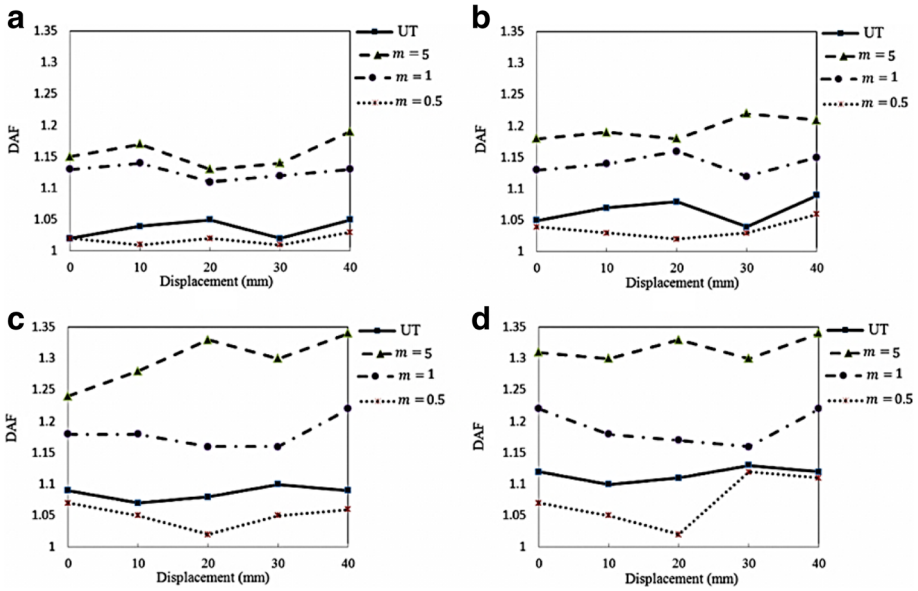

Fig. 15 The effect of impact velocity on DAF for UT and FGT with various exponent gradient *m*. **a** $v = 5m/s$. **b** $v = 10m/s$. **c** $v = 20m/s$. **d** $v = 30m/s$

space. Furthermore, the overall efficiency coefficient $F_g = 1$ indicates the optimal solution and $F_g = 0$ corresponds to the worst solution. In this paper, f_1 is the DAF(m, r), f_2 is $P_{\max}$ (m, r), and x_1, x_2, respectively, are the design variables m and r.

It must be emphasized that in order to optimize the two DAF(m, r) and P_{max} (m, r) objectives by the geometrical average method, the $F_g(m, r)$ is maximized and for the best design, the values of d_{DAF} and d_P are required to be as large as possible. The efficiency cost function $F_g(m, r)$ vs. design variables m and r are displayed in Fig. 16. It is observed that the shape of cost function is varied by changing the design variable. The optimization data which are obtained from the geometrical average method are tabulated in Table 7. The results yielded from the optimization indicate that the FGT inversion is superior to its counterparts ("Design optimization of DAF for coefficient of friction μ_d and exponent gradient m" section) in overall crashworthiness.

Conclusions

In this paper, a new type of structure called functionally graded thickness inversion tubes subjected to axial loading has been investigated by employing finite element code LS-DYNA. Energy absorption response was quantified with respect to variations in the parameter of die radius, coefficient of friction, and tube thickness variation pattern. The results have demonstrated the feasibility and superior performance of FGT tubes with optimum design variables as energy absorbers. Some optimization tools such as the weighted average method and multi-

Table 6 Optimum die radius r and exponent gradient m obtained through MDO for FGT inversion tube

Number of cycle	Design parameter interval	Optimal exponent gradient m	Optimal die radius r (mm)	DAF	$P_{\max}$ (kN)
1	$3 < m < 4$ $0.01 < \mu_d < 0.02$	4	0.02	1.2	59.66
2	$4 < m < 5$ $0.02 < \mu_d < 0.03$	4.8	0.028	1.3	57.34
3	$5 < m < 6$ $0.03 < \mu_d < 0.04$	5.7	0.031	1.4	52.23
4	$6 < m < 8$ $0.03 < \mu_d < 0.035$	6.3	0.031	1.5	50.42
5	$6 < m < 7$ $0.03 < \mu_d < 0.033$	6.1	0.033	1.5	50.01

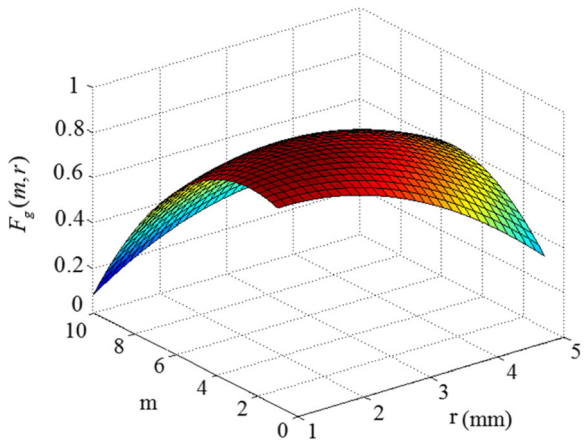

Fig. 16 The efficiency cost function $F_g(m, r)$ vs. design variables m and r

design objective technique utilized to optimize the FGT inversion tubes. The primary conclusions and design information this study outlined as follows:

(1) Sensitivity analysis indicates that several design parameters (die radius r, coefficient of friction μ_d, tube thickness variation pattern) have significant effect on SEA and peak force, which justify the selection of these parameters in multi-objective optimization.
(2) Friction between the die-tube interfaces plays a key role in the overall development of inversion process. In fact, a successful inversion mode of deformation easily switches into an unacceptable mode by simply changing this parameter. Optimization results show that the reduction of friction coefficient to less than 0.04 during inversion leads to the drastic improvement of crashworthiness performance.
(3) Experimental and numerical results present that the peak load in FGT inversion tubes obviously decreases, and simultaneously the load level increases steadily.
(4) The results achieved from multi-objective crashworthiness optimization show that using concave function for thickness distribution of tubes improves SEA without significant growth of initial peak force.
(5) The nonlinear thickness distribution exponent gradient m and die radius r are important parameters to control the DAF of FGT inversion response under dynamic loading. The optimum DAF of FGT inversion tube has different behavior and it increases at the dynamic deformation.

Table 7 Optimum die radius and gradient thickness obtained through the geometrical average method

Optimal values	$F_g(m, r)$	d_{DAF}		DAF	P_{max} (kN)
$m = 6.4$, μ_d=.034	0.7358	0.8451	0.8342	1.75	44.32

Briefly, this research introduces new designs of inversion tubes as energy absorber with superior characteristics with respect to UT tubes, under uniaxial loading. The multi-objective optimization method introduced here gives valuable information to develop and design of FGT inversion tubes in applications involving crush loading, such as automotive, aerospace, transportation, and defense industries.

Authors' contributions
Both authors read and approved the final manuscript.

Received: 2 August 2016 Accepted: 15 September 2016
Published online: 27 September 2016

References

Ahmad, Z., & Thambiratnam, D. (2009a). Application of foam-filled conical tubes in enhancing the crashworthiness performance of vehicle protective structures. *International Journal of Crashworthiness, 14*(4), 349–363.
Ahmad, Z., & Thambiratnam, D. P. (2009b). Dynamic computer simulation and energy absorption of foam-filled conical tubes under axial impact loading. *Computers & Structures, 87*(3–4), 186–197.
Ahmad, Z., & Thambiratnam, D. P. (2009c). Crushing response of foam-filled conical tubes under quasi-static axial loading. *Materials and Design, 30*(7), 2393–2403.
Aktay, L., Kröplin, B. H., Toksoy, A. K., & Güden, M. (2008). Finite element and coupled finite element/smooth particle hydrodynamics modeling of the quasi-static crushing of empty and foam-filled single, bi tubular and constraint hexagonal- and square-packed aluminum tubes. *Materials and Design, 29*(5), 952–962.
Al-Hassani, S. T. S., Johnson, W., & Lowe, W. T. (1972a). Characterization of inversion tubes under axial loading. *Journal of Mechanical Engineering Sciences, 14*, 370–381.
Al-Hassani, S. T. S., Johnson, W., & Lowe, W. (1972b). Characteristics of inversion tubes under axial loading. *Journal of Mechanical Engineering Science, 14*, 370–381.
ASTM Standard E8/E8M-08. (2003). *Standart test methods for tension testing of metallic materials*. PA, West Conshohocken: ASTM international.
Bisagni C. Crashworthiness of helicopter subfloor structures. Int J Impact Eng 27(10):1067–82.
Chirwa, E. C. (1993). Theoretical analysis of tapered thin-walled metal inverbuck tube. *International Journal of Mechanical Sciences, 35*(3-4), 325–351.
Colokoglu, A., & Reddy, T. Y. (1996). Strain rate and inertial effects in free external inversion of tubes. *International Journal of Crashworthiness, 1*(1), 93–106.
Guist LR, Marble DP (1966) Prediction of the inversion load of a circular tube. NASATND 3622.
Hanssen, A. G., Langseth, M., & Hopperstad, O. S. (2000). Static and dynamic crushing of square aluminium extrusions with aluminium foam filler. *International Journal of Impact Engineering, 24*(4), 347–383.
Hou, S. J., Li, Q., Long, S. Y., Yang, X. J., & Li, W. (2008). Multiobjective optimization of multi-cell sections for the crashworthiness design. *International Journal of Impact Engineering, 35*(11), 1355–1367.
Karagiozova, D., Alves, M., & Jones, N. (2000). Inertia effects in axisymmetrically deformed cylindrical shells under axial impact. *International Journal of Impact Engineering, 24*, 1083–1115.
Liao, X. T., Li, Q., Yang, X. J., Zhang, W. G., & Li, W. (2008). Multiobjective optimization for crash safety design of vehicles using stepwise regression model'. *Struct. Multidisc. Optim., 35*, 561–569.
Marsolek, J., & Reimerdes, H. (2002). Energy absorption of metallic cylindrical shells with induced non-axisymmetric folding patterns. *International Journal of Impact Engineering, 30*(8), 1209–1223.
Masmoudi, M., Ketata, H., & Krichen, A. (2016). External curling process of thin tubes: finite element and experimental investigation. *International Journal of Advanced Manufacturing Technology*. doi:10.1007/s00170-016-8742-x.

Miller, W. S., Zhuang, L., Bottema, J., Wittebrood, A. J., De Smet, P., & Haszler, A. (2000). Recent development in aluminium alloys for the automotive industry. *Materials Science and Engineering A, 280*, 37–49.
Mirfendereski, L., Salimi, M., & Ziaei-Rad, S. (2008). Parametric study and numerical analysis of empty and foam-filled thin-walled tubes under static and dynamic loadings. *International Journal of Mechanical Sciences, 50*(6), 1042–1057.
Miscow, P. C., & AL-Qureshi, H. A. (1997). Mechanics of static and dynamic inversion processes. *International Journal of Mechanical Sciences, 39*, 147–161.
Mohammadiha, O., & Ghariblu, H. (2016). Crush behavior optimization of multi-tubes filled by functionally graded foam. *Thin Walled Structures, 98*, 627–639.
Qiao, P. Z., Yang, M. J., & Mosallam, A. S. (2004). Impact analysis of I-Lam sandwich system for over-height collision protection of highway bridges. *Engineering Structures, 26*, 1003–1012.
Reddy, T. Y. (1992). Guist and Marble revisited—on the natural knuckle radius in tube inversion. *International Journal of Mechanical Sciences, 34*(10), 761–768.
Saleh ghaffari, S., Tajdari, M., Panahi, M., & Mokhtarnezhad, F. (2010). Attempts to improve energy absorption characteristics of circular metal tubes subjected to axial loading. *Thin Walled Structures, 48*(6), 379–390.
Sun, G. Y., Li, G. Y., Hou, S. J., Zhou, S. W., Li, W., & Li, Q. (2010). Crashworthiness design for functionally graded foam-filled thin-walled structures. *Materials Science and Engineering A, 527*(7–8), 1911–1919.
Zarei, H., & Kroger, M. (2008). Optimum honeycomb filled crash absorber design. *Materials and Design, 29*(1), 193–204.
Zhang, X., & Huh, H. (2009). Energy absorption of longitudinally grooved square tubes under axial compression. *Thin Walled Structures, 47*(12), 1469–1477.
Zhang, X., & Zahng, H. (2015). Relative merits of conical tubes with graded thickness subjected to oblique impact loads. *International Journal of Mechanical Sciences, 98*, 111–125.
Zhang, X., & Zhang, H. (2013). Energy absorption of multi-cell stub columns under axial compression. *Thin Walled Structures, 68*, 156–163.
Zhang, X., & Zhang, H. (2014). Axial crushing of circular multi-cell columns. *International Journal of Impact Engineering, 65*, 110–125.
Zhang, X., Cheng, G., You, Z., & Zhang, H. (2007). Energy absorption of axially compressed thin-walled square tubes with patterns. *Thin Walled Structures, 45*(9), 737–746.